ELSEVIER

A peridynamic model of flow in porous media

CrossMark

Rami Jabakhanji [a,*], Rabi H Mohtar [b,c]

[a] Department of Agricultural and Biological Engineering, Purdue University, West Lafayette, IN, USA
[b] Department of Biological and Agricultural Engineering, Texas A&M University, College Station, TX, USA
[c] Zachry Department of Civil Engineering, Texas A&M University, College Station, TX, USA

ARTICLE INFO

ABSTRACT

This paper presents a nonlocal, derivative free model for transient flow in unsaturated, heterogeneous, and anisotropic soils. The formulation is based on the peridynamic model for solid mechanics. In the proposed model, flow and changes in moisture content are driven by pairwise interactions with other points across finite distances, and are expressed as functional integrals of the hydraulic potential field. Peridynamic expressions of the rate of change in moisture content, moisture flux, and flow power are derived, as are relationships between the peridynamic and the classic hydraulic conductivities; in addition, the model is validated. The absence of spacial derivatives makes the model a good candidate for flow simulations in fractured soils and lends itself to coupling with peridynamic mechanical models for simulating crack formation triggered by shrinkage and swelling, and assessing their potential impact on a wide range of processes, such as infiltration, contaminant transport, and slope stability.

© 2015 Elsevier Ltd. All rights reserved.

1. Introduction

Naturally occurring soils, especially fine-textured ones, exhibit shrinking and swelling behavior [1–3]. These soils tend to swell when their moisture content increases, and shrink when it decreases. At the field scale, this behavior leads to tensile stresses that may exceed the soil's failure limit and trigger the formation and evolution of cracks during drying phases. Cracks may in turn close during infiltration phases when the soil becomes wetter and swells [4–6] giving them a dynamic nature leading to highly nonlinear responses. These desiccation cracks have a length scale of ten to a hundred centimeters and their effect on the hydraulic properties of the soil is not captured by standard laboratory tests using a Representative Elementary Volume (REV) with a length scale of a few centimeters.

Desiccation cracking has a wide spectrum of environmental, agricultural, and hydrological impacts. The movement of moisture and solutes into and within the soil increases due to the presence of these cracks that act as preferential pathways for rapid water movement to deeper layers [7–11]. This rapid movement may lower the effectiveness of irrigation [12] and causes fast seepage of nutrients and pesticides away from the plants into deeper layers reducing the contaminants' residence time in the unsaturated zone where they are usually absorbed by the plants and degraded by

bacteria, and increasing the probability of ground water and/or surface water contamination, depending on the relief. In addition, desiccation cracks can have a dramatic effect on processes of surface water movement and flood dynamics by altering the partitioning of rainfall between infiltration and runoff, which is an important issue to consider when modeling and forecasting flood events.

Desiccation cracks also have engineering and geotechnical impacts with potentially very serious environmental and public safety repercussions. For example, desiccation cracks developing at the surface of a slope may trigger the onset of a landslide. If they develop in the core of an earth dam, cracks act as preferential moisture flow paths, increasing the moisture content of the dam and, with it, the pore water pressure which eventually leads to its failure [13]. Clay barriers used in landfills and nuclear waste disposal sites are also subject to desiccation cracking which reduces the barrier's containment effectiveness [14,15].

In this paper, we present a peridynamic model for transient moisture flow in unsaturated, heterogeneous, and anisotropic soils. The model is an alternative to the classic Richard's equation and is based on Silling's reformulation of the theory of elasticity for solid mechanics [16,17]. In the proposed model, we replace the classic, local, continuum mechanics formulation by a nonlocal integral functional. The model is free of spacial derivatives, and the flow is driven by the hydraulic potential field instead of the gradient of the hydraulic potential field. Katiyar et al. [18] have derived similar peridynamic formulations for saturated steady state flow.

* Corresponding author.
    E-mail addresses: rjabakha@purdue.edu (R. Jabakhanji), mohtar@tamu.edu (R.H Mohtar).

Due to the lack of spacial derivatives, this model is capable of handling the spurious formation of cracks, which translate into points of singularities in the parameter and hydraulic potential fields, within the simulation domain without failing. This would allow us to couple the derived model with a peridynamic mechanical model and simulate the formation of desiccation cracks and their dynamics and assess the potential of such an approach on evaluating their impact on flow and solute transport. This coupling is however the subject of a subsequent paper.

We would like to point out that the nonlocal aspect of the proposed model is related to the mechanism of state change in the domain. In classic nonlocal formulations [19–25], the new value of a state is the one with the maximum likelihood and the change is driven by some statistical measure of the gradient of the driving field within the surrounding region. On the other hand, in peridynamic models such as this one, the change of state at a point is driven by the influence of the value of some field at points that are at some finite distance away.

We will start by presenting the peridynamic model concept and derive the peridynamic expression for the rate of change of moisture content. We will then derive the peridynamic equations of flow power dissipation and moisture flux, which we will use in deriving the relationship between the peridynamic hydraulic conductivity density and the classic hydraulic conductivity for unsaturated, homogeneous, heterogeneous, isotropic, and anisotropic soils. We will also show that the peridynamic model equations of moisture flow and flux converge to the classic Richard's and Darcy's equations at the limit of vanishing horizon. This will be followed by a presentation of the numerical implementation and validation of the model in one and two dimensions.

2. Peridynamic flow model

Consider the homogeneous and isotropic body of soil Ω in Fig. 1, where each point $\mathbf{x}$ in Ω represents a differential volume dV_x [L^3], and is at some total hydraulic potential $H(\mathbf{x})$ [L]. Suppose the change in moisture content at every point $\mathbf{x}$ in Ω is driven by pairwise interactions with all other points $\mathbf{x}'$ in Ω despite the finite distance separating each pair points.

Suppose also that these pairwise interactions are equivalent to a one dimensional resistive pipe that acts as a conduit and does not store any moisture, that we will call peripipe, and that each peripipe has a property called the peridynamic hydraulic conductance density, $C(\mathbf{x}, \mathbf{x}')$ [$T^{-1}L^{-4}$], which is equal to the volume of moisture that will flow per second in peripipe $\mathbf{xx}'$ per unit hydraulic potential difference, per unit volume of $\mathbf{x}$, and per unit volume of $\mathbf{x}'$.
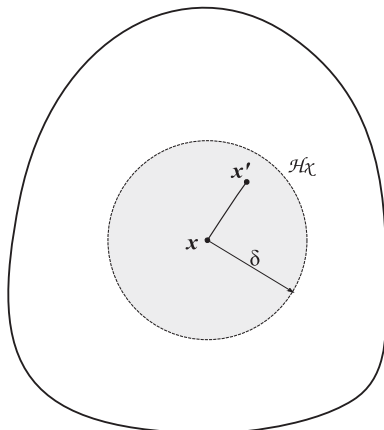

Fig. 1. Peridynamic medium representation. Point $\mathbf{x}$ is influenced by all points within its horizon. $\mathcal{H}_x$ is the horizon of $\mathbf{x}$, δ is the radius of the horizon.

We can now define the pairwise interaction which we will call the peridynamic flow density function $J(\mathbf{x}, \mathbf{x}')$ [$T^{-1}L^{-3}$], as the rate of moisture flow from point $\mathbf{x}'$ to point $\mathbf{x}$ per unit volume of $\mathbf{x}$ per unit volume of $\mathbf{x}'$:

$$J(\mathbf{x}, \mathbf{x}') = C(\mathbf{x}, \mathbf{x}')[H(\mathbf{x}') - H(\mathbf{x})], \tag{1}$$

where the peripipe conductance $C(\cdot)$ is calculated from the peridynamic hydraulic conductivity density, $\kappa(\mathbf{x}', \mathbf{x})$ [$T^{-1}L^{-3}$], an intrinsic material property which is not equal to, but can be related to the classic hydraulic conductivity K [LT^{-1}].

$$C(\mathbf{x}, \mathbf{x}') = \frac{\kappa(\mathbf{x}', \mathbf{x})}{\|\mathbf{xx}'\|}. \tag{2}$$

The change of moisture stored at $\mathbf{x}$, and that of point $\mathbf{x}'$ mediated by peripipe $\mathbf{xx}'$, $\Delta V_m(\mathbf{x}, \mathbf{x}')$ [L^3], and $\Delta V_m(\mathbf{x}', \mathbf{x})$ [L^3] respectively are given by:

$$\Delta V_m(\mathbf{x}, \mathbf{x}') = \kappa(\mathbf{xx}')\frac{[H(\mathbf{x}') - H(\mathbf{x})]}{\|\mathbf{xx}'\|}dV_{x'}dV_x, \tag{3}$$

$$\Delta V_m(\mathbf{x}', \mathbf{x}) = \kappa(\mathbf{x}'\mathbf{x})\frac{[H(\mathbf{x}) - H(\mathbf{x}')]}{\|\mathbf{x}'\mathbf{x}\|}dV_xdV_{x'}. \tag{4}$$

Because peripipes do not store any moisture, and due to conservation of mass we have $\Delta V_m(\mathbf{x}, \mathbf{x}') = -\Delta V_m(\mathbf{x}', \mathbf{x})$, and because $\|\mathbf{xx}'\| = \|\mathbf{x}'\mathbf{x}\|$, we get the following restriction on $\kappa(\cdot)$:

$$\kappa(\mathbf{x}', \mathbf{x}) = \kappa(\mathbf{x}, \mathbf{x}'). \tag{5}$$

Using Eq. (1), the total change in volumetric moisture content at any point $\mathbf{x}$ in Ω due to its interaction with all other points $\mathbf{x}'$ in Ω, in addition to external sources, or sinks, of moisture at point $\mathbf{x}, S(x)$ [T^{-1}] is given by the following functional integral:

$$\frac{\partial \theta}{\partial t}(\mathbf{x}) = \int_\Omega \kappa(\mathbf{x}, \mathbf{x}')\frac{[H(\mathbf{x}') - H(\mathbf{x})]}{\|\mathbf{xx}'\|}dV_{x'} + S(x), \quad [T^{-1}]. \tag{6}$$

Eq. (6) is the peridynamic equation of flow for unsaturated porous media. Note that there are no restrictions on $C(\cdot, \cdot)$ beyond the one stated in Eq. (5) and being integrable. Integrating this equation over the entire domain Ω, we get the total change of moisture in the domain:

$$\int_\Omega \frac{\partial \theta}{\partial t}(\mathbf{x})dV_x = \int_\Omega \int_\Omega \kappa(\mathbf{x}, \mathbf{x}')\frac{[H(\mathbf{x}') - H(\mathbf{x})]}{\|\mathbf{xx}'\|}dV_{x'}dV_x$$
$$+ \int_\Omega S(x)dV_x, \quad [L^3]. \tag{7}$$

Rewriting the first integral in the right hand side as follows:

$$\int_\Omega \int_\Omega \frac{\kappa(\mathbf{x}', \mathbf{x})H(\mathbf{x}')}{\|\mathbf{xx}'\|}dV_{x'}dV_x - \int_\Omega \int_\Omega \frac{\kappa(\mathbf{x}', \mathbf{x})H(\mathbf{x})}{\|\mathbf{xx}'\|}dV_{x'}dV_x, \tag{8}$$

and switching the variables x and x' in the second integral and reversing the integration order while keeping in mind the restriction on $C(\cdot, \cdot)$ (Eq. (5)), we realize that Eq. (8) evaluates to zero, and Eq. (7) becomes:

$$\int_\Omega \frac{\partial \theta}{\partial t}(\mathbf{x})dV_x = \int_\Omega S(x)dV_x. \tag{9}$$

Eq. (9) is a statement of conservation of mass in the domain and it states that the total change in moisture content in the domain Ω is equal to the total amount of moisture added, or removed from external sources.

We will now introduce an additional property of a peridynamic medium, which is that any two points $\mathbf{x}$ and $\mathbf{x}'$ separated by a distance greater than a maximum distance δ are too far apart to interact. For every point $\mathbf{x}$ in Ω we will define the horizon of $\mathbf{x}$ as the set

$\mathcal{H}_x$ of all points $\mathbf{x}'$ in Ω that lie within a distance δ of $\mathbf{x}$. We will call δ the radius of the horizon, and $\mathbf{x}$ the center of the horizon:

$$\mathcal{H}_x = \{\mathbf{x}' \in \Omega \mid 0 \leqslant \|\mathbf{x}' - \mathbf{x}\| \leqslant \delta\}. \tag{10}$$

Rewriting Eq. (6) to reflect this new proposition, we get:

$$\frac{\partial \theta}{\partial t}(\mathbf{x}) = \int_{\mathcal{H}_x} \kappa(\mathbf{x}, \mathbf{x}') \frac{[H(\mathbf{x}') - H(\mathbf{x})]}{\|\mathbf{x}\mathbf{x}'\|} dV_{x'} + S(x), \quad [T^{-1}]. \tag{11}$$

In one dimension, where dx' is the one-dimensional equivalent of $dV_{x'}$, Eq. (6) becomes:

$$\frac{\partial \theta}{\partial t}(x) = \int_{x-\delta}^{x+\delta} \frac{\kappa(\mathbf{x}, \mathbf{x}')(H(\mathbf{x}') - H(\mathbf{x}))}{\|\mathbf{x}\mathbf{x}'\|} dx'. \tag{12}$$

And in two dimensions, where it is simpler to write Eq. (6) in a polar coordinate system centered at point $\mathbf{x}$, and where $rdrd\theta$ is the two-dimensional equivalent of $dV_{x'}$, and $r = \|\mathbf{x}\mathbf{x}'\|$ Eq. (6) becomes:

$$\frac{\partial \theta}{\partial t}(\mathbf{x}) = \int_0^{2\pi} \int_0^{\delta} \kappa(\mathbf{x}, \mathbf{x}')(H(\mathbf{x}') - H(\mathbf{x})) dr d\theta, \tag{13}$$

with:

$$\mathbf{x} = (0,0), \quad \mathbf{x}' = (r, \theta).$$

It can be observed that Eqs. (6)–(13) do not depend on any spacial derivatives and are therefore valid everywhere in the domain including discontinuities of parameters $(\kappa(\cdot, \cdot))$ and hydraulic potential field $(H(\cdot))$. Whereas the classic Richard's equation (Eq. (14)) depends on spacial derivatives of the hydraulic conductivity and the hydraulic potential $(\frac{\partial H(x)}{\partial x}, \frac{\partial^2 H(x)}{\partial x^2}, \frac{\partial K(x)}{\partial x})$ and to be valid everywhere in the domain requires that the hydraulic conductivity field be differentiable and the hydraulic potential be twice differentiable. If the model were coupled with a peridynamic mechanical model, soil volumetric changes due to moisture change would be evaluated using a soil shrinkage curve and fed into the mechanical submodel for evaluation. If these changes result in some links (peripipes) exceeding the soil failure limit, those links would be severed affecting the subsequent deformation of the soil and moisture flow. This is captured by multiplying the flow density function by a test function that reduces to zero if the interaction is severed, otherwise it is one.

$$\frac{\partial \theta}{\partial t} = K \frac{\partial^2 H}{\partial x^2} + \frac{\partial K}{\partial x} \frac{\partial H}{\partial x}. \tag{14}$$

3. Flow power and moisture flux

We will now define the peridynamic expressions for moisture flux, and for the power dissipated by moisture flow. These are important quantities in analyzing flow problems in general, and are particularly useful in deriving the relationship between the peridynamic hydraulic conductivity κ and the classic conductivity K. We will use the peridynamic equation for moisture flux during our derivation of the relationship between κ and the classic conductivity K for the case of one-dimensional flow, and the peridynamic flow power to derive the κ-K relationship for the two-dimensional, isotropic and anisotropic flow case.

3.1. Moisture flux

In peridynamic terms, moisture flux at any point $\mathbf{x}$ across a surface S along its normal direction $\mathbf{S}_\perp$ is the net volume of moisture exchanged between points located on one side of S with points located on the other side of S per unit time per unit area. The component normal to S of the flow through a peripipe $\mathbf{x}\mathbf{x}'$ is given by:

$$J_\perp(\mathbf{x}, \mathbf{x}') = J(\mathbf{x}, \mathbf{x}') \frac{\mathbf{x}\mathbf{x}'}{\|\mathbf{x}\mathbf{x}'\|} \cdot \mathbf{S}_\perp. \tag{15}$$

Now assume that the horizon of a point $\mathbf{x}$ located on S is divided by this surface into a set of points located below S, and another set of points above it (Fig. 2). We will refer to these sets by $\mathcal{H}_x^l$ and $\mathcal{H}_x^u$ respectively.

$$\mathcal{H}_x^u = \{\mathbf{x}_u \in \mathcal{H}_x \mid (\mathbf{x}\mathbf{x}_u) \cdot \mathbf{S}_\perp > 0\}, \tag{16}$$

$$\mathcal{H}_x^l = \{\mathbf{x}_l \in \mathcal{H}_x \mid \mathbf{x}_l \notin \mathcal{H}_x^u\}. \tag{17}$$

For each point $\mathbf{x}_l \in \mathcal{H}_x^l$ we want the set of points that interact with it, which are the points at a maximum distance δ; we also want them to be on the other side of S, which means they belong to $\mathcal{H}_x^u$, and we require that the peripipe passes through point $\mathbf{x}$. This set is defined as follows:

$$\mathcal{H}_{x_l}^u = \{\mathbf{x}_l' \in \mathcal{H}_x^l \mid \|\mathbf{x}_l\mathbf{x}_l'\| \leqslant \delta, \quad \mathbf{x}_l\mathbf{x}_l' \times \mathbf{x}_l\mathbf{x} = 0\}. \tag{18}$$

Summing up all of these interaction leads to the value of the moisture flux across point x:

$$q_{\perp S}(\mathbf{x}) = -\int_{\mathcal{H}_{x_l}^u} \int_{\mathcal{H}_x^l} J_\perp(\mathbf{x}_l\mathbf{x}_l') dV_{x_l} dV_{x_l'}, \quad [LT^{-1}]. \tag{19}$$

In one-dimension, Eq. (19) becomes:

$$q(\mathbf{x}) = -\int_{x-\delta}^{x} \int_{x}^{x'+\delta} \frac{\kappa(\mathbf{x}, \mathbf{x}')(H(x'') - H(x'))}{\|\mathbf{x}'\mathbf{x}''\|} dx' dx''. \tag{20}$$

In two dimensions, the equation for the flux in polar coordinates across $x = (0, 0)$, and normal to the surface S with angle ϕ is:

$$q(\phi) = \int_{\pi}^{2\pi} \int_0^{\delta-r'} \int_{\delta}^{0} \kappa(\mathbf{x}, \mathbf{x}')(H(x'') - H(x')) \sin(\theta + \phi) dr' dr'' d\theta, \tag{21}$$

with:

$$\mathbf{x}' = (r', \theta), \quad \mathbf{x}'' = (r'', \theta - \pi).$$

Here we can also note that Eqs. (20) and (21) do not depend on any spacial derivatives and are valid everywhere in the domain including discontinuities the hydraulic potential field $(H(\cdot))$. Whereas, The classic Darcy's equation (Eq. (22)) depends on spacial derivatives of the hydraulic potential $(\frac{\partial H(x)}{\partial x})$ and to be valid everywhere in the domain requires that the hydraulic potential field be differentiable.

$$q(\mathbf{x}) = K \frac{\partial H(\mathbf{x})}{\partial x}. \tag{22}$$

3.2. Flow power

In the peridynamic flow model, we will define the power dissipated by moisture flow at point $\mathbf{x}$ as the power dissipated by the flow mobilized due to $\mathbf{x}$, which is equal to half of the power
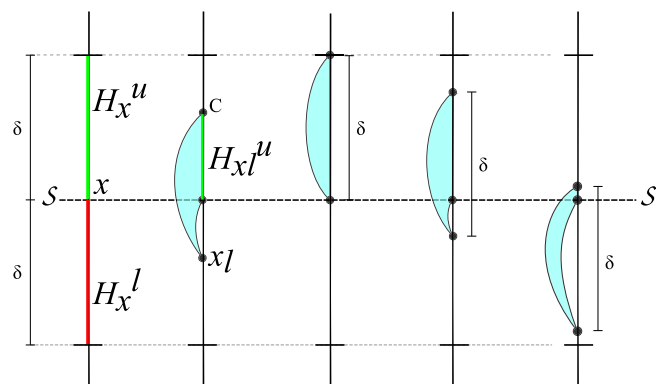

Fig. 2. One-dimensional moisture flux.

dissipated in all peripipes connected to $\mathbf{x}$, the other half being the sum of the shares of the second point in each interaction.

For each peripipe let us define the peridynamic power density function as the power dissipated per unit volume squared, which is equal to the flow density function times the hydraulic potential difference:

$$P_p(\mathbf{x}, \mathbf{x}') = \frac{\kappa(\mathbf{x}, \mathbf{x}') \left(H(\mathbf{x}') - H(\mathbf{x}) \right)^2}{\|\mathbf{x}\mathbf{x}'\|}, \quad [\mathrm{L}^{-2}\mathrm{T}^{-1}]. \tag{23}$$

Dividing Eq. (23) by two to get the share of $\mathbf{x}$, then multiplying by the volume of $\mathbf{x}'$ and integration over the entire horizon $\mathcal{H}_x$ gives us the volumetric power dissipation at point $\mathbf{x}$:

$$P(\mathbf{x}) = \frac{1}{2} \int_{\mathrm{H}_x} \frac{\kappa(\mathbf{x}, \mathbf{x}') \left(H(\mathbf{x}') - H(\mathbf{x}) \right)^2}{\|\mathbf{x}\mathbf{x}'\|} dV_{x'}, \quad [\mathrm{LT}^{-1}]. \tag{24}$$

The forms of Eq. (24) in one dimension and two dimensions are given by Eqs. (25) and (26) respectively.

$$P(\mathbf{x}) = \frac{1}{2} \int_{x-\delta}^{x+\delta} \frac{\kappa(\mathbf{x}, \mathbf{x}') \left(H(\mathbf{x}') - H(\mathbf{x}) \right)^2}{\|\mathbf{x}\mathbf{x}'\|} dx', \tag{25}$$

$$P(\mathbf{x}) = \frac{1}{2} \int_0^{2\pi} \int_0^{\delta} \kappa(\mathbf{x}, \mathbf{x}') \left(H(\mathbf{x}') - H(\mathbf{x}) \right)^2 dr d\theta, \tag{26}$$

with:

$$\mathbf{x} = (0,0), \quad \mathbf{x}' = (r, \theta).$$

4. Peridynamic hydraulic conductivity

In this section we would like to relate the non-measurable peridynamic hydraulic conductivity to the classic hydraulic conductivity of the soil. This entails finding an expression for κ as a function of the classic hydraulic conductivity that results in equal values for variables such as moisture flux or flow power in the peridynamic and classic model.

So far, the only parameter influencing the degree of locality of the model is δ, the radius of the horizon. The smaller δ is, the more local the model is, and vice versa. In addition, all the points within a horizon have an equal influence on its center; the distance to the center being only an argument of the conductance of a peripipe and having no influence on the attenuation of the potential felt at the center. We would like to lift this limitation by introducing a dependence of the influence of one point on another on the distance separating them. This adds an extra feature to the description of nonlocality which expands the range of behavior captured by the model.

4.1. Influence functions

Several influence function types have been used in peridynamic formulations to describe the dependence of the pairwise interaction on the separation distance. The simplest influence function is constant, or uniform; it shows no additional dependence on the separation distance [16,17,26,27]. In evaluating the role the shape of the influence function plays on the behavior of a peridynamic model, Seleson and Parks used a family of spherical influence functions with a softening length of the form $f_p(r) = (r + \epsilon)^{-p}$ [28]. Kilic and Madenci [29] used a normal distribution in their peridynamic thermomechanical model derivation. In our derivation we used two types of influence functions. The first is a uniform function; the second is a linear one.

For the case of a uniform influence function (Fig. 3(a)), there is no dependence of the peridynamic hydraulic conductivity on the distance between points, and peridynamic conductivity function is constant:

$$\kappa(\mathbf{x}, \mathbf{x}') = \kappa. \tag{27}$$

For the case of a linear influence function (Fig. 3(b)), the peridynamic hydraulic conductivity function $\kappa(\mathbf{x}, \mathbf{x}')$ has a maximum at the center of the horizon and it decreases linearly as the length of the peripipe increases. If we set the influence to be zero at the edge of the horizon and one at the center we get:

$$\kappa(\mathbf{x}, \mathbf{x}') = \kappa \left(1 - \frac{\|\mathbf{x}\mathbf{x}'\|}{\delta} \right). \tag{28}$$

4.2. One-dimensional conductivity

In this section, we will derive the peridynamic hydraulic conductivity function for the simple case of isotropic soils. Suppose we have a saturated one-dimensional infinite homogeneous soil column. Suppose also that the column is at steady state and under a linear hydraulic potential field $H(x) = ax + c$. We would like to have the moisture flux across a surface perpendicular to the column at x_s given by the classic method to be equal to the same given by the peridynamic flow model.

According to the classic formulation, the flux at x_s is given by Darcy's Law:

$$\mathbf{q}(x_s) = -Ka, \tag{29}$$

where K is the classic hydraulic conductivity and a is the applied hydraulic potential gradient. According to the peridynamic formulation, the flux across the surface is given by:

$$\mathbf{q}(x_s) = -\int_{x_s-\delta}^{x_s} \int_{x_s}^{x''+\delta} a\,\kappa(\mathbf{x}\mathbf{x}') dx' dx''. \tag{30}$$

In the case of a uniform influence function where $\kappa(\mathbf{x}, \mathbf{x}') = \kappa$, solving the integral in Eq. (30) results in the following:

$$\mathbf{q}(\mathbf{x_s}) = -\frac{\kappa a \delta^2}{2}. \tag{31}$$

Equating Eqs. (31) and (29) leads to the following relationship between the classic hydraulic conductivity and the peridynamic hydraulic conductivity:

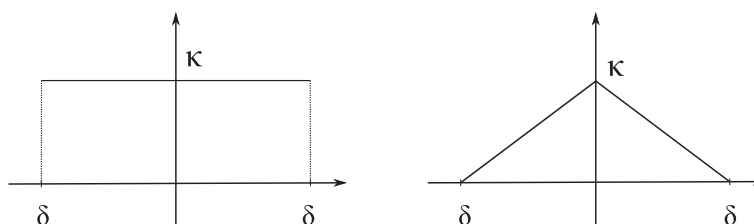$$\kappa(\mathbf{x}, \mathbf{x}') = \frac{2K}{\delta^2}. \tag{32}$$

Fig. 3. Uniform and linear influence functions.

In the case of a linear influence function, we plug Eq. (28) in Eq. (30), solve the integral and equate the result with Eq. (29) and get:

$$\kappa(\mathbf{x}, \mathbf{x}') = \frac{6K}{\delta^2}\left(1 - \frac{\|\mathbf{xx}'\|}{\delta}\right). \tag{33}$$

4.3. Two-dimensional isotropic conductivity

We will now derive the isotropic hydraulic conductivity function in two dimensions. In this case, for ease of demonstration we will equate expressions of flow power instead of flux. Consider a two dimensional saturated soil column at steady state subject to a linear hydraulic potential $H(\mathbf{x}) = a\mathbf{x} \cdot \hat{j} + c$. In the classical local continuum framework, the power dissipated by moisture flow through an infinitesimal element at point $\mathbf{x}$ for this case is given by:

$$P(\mathbf{x}) = \frac{1}{2}a^2 K. \tag{34}$$

The expression for power in the peridynamic framework in two dimensions is given by Eq. (26). Having a linear hydraulic potential, we can write the following expression for the potential difference in polar coordinates:

$$H(\mathbf{x}') - H(\mathbf{x}) = a r \sin(\theta), \tag{35}$$

with:

$$\mathbf{x} = (0, 0), \quad \mathbf{x}' = (r, \theta).$$

Eq. (26) becomes:

$$P(\mathbf{x}) = \frac{1}{2}\int_0^{2\pi}\int_0^{\delta}\kappa(\mathbf{x}, \mathbf{x}')a^2 r^2 \sin(\theta)^2\,dr d\theta. \tag{36}$$

For the case of a uniform influence function, we replace $\kappa(\mathbf{x}, \mathbf{x}')$ by κ and we evaluate the integral in Eq. (36) and obtain:

$$P(\mathbf{x}) = \frac{a^2 \pi \delta^3}{12}\kappa. \tag{37}$$

Equating Eqs. (37) and (34) and solving for κ leads to the following relationship:

$$\kappa(\mathbf{x}, \mathbf{x}') = \frac{6}{\pi\delta^3}K. \tag{38}$$

For the case of a linear influence function, we replace $\kappa(\mathbf{x}, \mathbf{x}')$ by Eq. (28) in Eq. (36). After evaluating the integral, we equate with Eq. (34) and solve for κ and obtain the following:

$$\kappa(\mathbf{x}, \mathbf{x}') = \frac{24K}{\pi\delta^3}\left(1 - \frac{\|\mathbf{xx}'\|}{\delta}\right). \tag{39}$$

4.4. Two-dimensional anisotropic conductivity

We will now derive the equation for the peridynamic hydraulic conductivity function for the case of an anisotropic soil, where the hydraulic conductivity depends on the orientation θ of the peripipe.

Let the soil in a vertical column be anisotropic with $K_y = K$ and $K_x = nK$. In the classical framework, the power dissipated at $\mathbf{x}$ due to an applied uniform hydraulic gradient a in the direction of $\hat{j}$ is given by:

$$p(\mathbf{x}) = \frac{1}{2}a^2 K, \tag{40}$$

and the power dissipated at $\mathbf{x}$ due to an applied uniform hydraulic gradient a in the direction of $\hat{i}$ is given by:

$$p(\mathbf{x}) = \frac{1}{2}a^2 nK. \tag{41}$$

We need to derive an equation for $\kappa(\theta)$ that would yield a flow power equal to the classic formulation for both scenarios. In the classic framework, the directional hydraulic conductivity, $K(\theta)$, for an anisotropic medium is given by:

$$K(\theta) = \left(\frac{\cos^2(\theta)}{nK} + \frac{\sin^2(\theta)}{K}\right)^{-1}. \tag{42}$$

If we use the same form to express $\kappa(\theta)$ as a function of θ, we get different results when deriving the relationship between κ and the classic K by applying a uniform hydraulic potential gradient in the direction of $\hat{j}$ versus applying the gradient in the direction of $\hat{i}$. However, we will show by verification that the following relationship gives equal results.

$$\kappa(\theta) = \left(\frac{\cos^2(\theta)}{n^2 \kappa} + \frac{\sin^2(\theta)}{\kappa}\right)^{-1}. \tag{43}$$

For the case of a uniform influence function where $\kappa(\mathbf{xx}') = \kappa(\theta)$, the power dissipated at $\mathbf{x}$ due to a uniform hydraulic gradient a applied in the direction of $\hat{j}$ and then in the direction of $\hat{i}$ are given by Eqs. (44) and (45) respectively:

$$P_j(\mathbf{x}) = \frac{1}{2}\int_0^{\delta}\int_0^{2\pi}\kappa(\theta)a^2 r^2 \sin(\theta)^2\,dr d\theta, \tag{44}$$

$$P_i(\mathbf{x}) = \frac{1}{2}\int_0^{\delta}\int_0^{2\pi}\kappa(\theta)a^2 r^2 \cos(\theta)^2\,dr d\theta, \tag{45}$$

with:

$$\kappa(\theta) = \left(\frac{\cos^2(\theta)}{n^2 \kappa} + \frac{\sin^2(\theta)}{\kappa}\right)^{-1}.$$

Evaluating the integrals in Eqs. (44) and (45) leads to:

$$P_j(\mathbf{x}) = \frac{n\pi a^2 \delta^3}{3(n+1)}\kappa, \tag{46}$$

$$P_i(\mathbf{x}) = \frac{n^2 \pi a^2 \delta^3}{3(n+1)}\kappa. \tag{47}$$

Equating Eqs. (46) and (40), and solving for κ leads to:

$$\kappa = \frac{3(n+1)}{n\pi\delta^3}K. \tag{48}$$

Equating Eqs. (47) and (41), and solving for κ leads to the same result:

$$\kappa = \frac{3(n+1)}{n\pi\delta^3}K, \tag{49}$$

and the equation for the peridynamic hydraulic conductivity for an anisotropic soil in terms of the classic hydraulic conductivity K and the anisotropy ratio n using a uniform influence function is given by:

$$\kappa(\mathbf{x}, \mathbf{x}') = K\frac{3(n+1)}{n\pi\delta^3}\left(\frac{\cos^2(\theta)}{n^2} + \sin^2(\theta)\right)^{-1}. \tag{50}$$

If we use a linear influence function, we multiply the integrand in Eqs. (44) and (45) by the term $(1 - \|\mathbf{xx}'\|/\delta)$ and integrate to get the following:

$$P_j(\mathbf{x}) = \frac{n\pi a^2 \delta^3}{12(n+1)}\kappa, \tag{51}$$

$$P_i(\mathbf{x}) = \frac{n^2 \pi a^2 \delta^3}{12(n+1)}\kappa. \tag{52}$$

Equating Eqs. (51) and (52) with Eqs. (40) and (41) respectively leads to the same relationship given by:

$$\kappa = \frac{12(n+1)}{n\pi\delta^3}K,$$

(53)

and the equation for the peridynamic hydraulic conductivity for a homogeneous and anisotropic soil in terms of the classic hydraulic conductivity and the anisotropy ratio n for a linear influence function is given by:

$$\kappa(\mathbf{x},\mathbf{x}') = K\frac{12(n+1)}{n\pi\delta^3}\left(1 - \frac{\|\mathbf{xx}'\|}{\delta}\right)\left(\frac{cos^2(\phi)}{n^2} + sin^2(\phi)\right)^{-1}.$$

(54)

4.5. Generalizing to unsaturated, inhomogeneous soils

Eqs. (38), (39), (50), and (54) were derived under the assumption that the medium is homogeneous and at saturation, hence that it has a constant hydraulic conductivity. However, naturally occurring soils are almost always heterogeneous, and their hydraulic conductivity varies in space. In addition, even soils with fairly homogeneous parameters will exhibit spacial variability in their conductivity when in unsaturated regimes due to the dependence of the conductivity on the moisture content or matric potential.

In order to adapt the derivation to the general case of inhomogeneous soils in the unsaturated regime, we will modify the mechanics of pairwise interactions and make additional assumptions. We will first replace each peripipe by two parallel peripipes, each responsible for half the interaction of the original one, and each has the peridynamic hydraulic conductivity of one of the nodes. We will also assume that the relationship between the peridynamic and the classic hydraulic conductivity is independent of the distribution of the moisture content within the horizon. With these modifications, the peridynamic hydraulic conductivity density is now given by:

$$\kappa(\mathbf{x},\mathbf{x}') = \frac{\kappa(\mathbf{x}) + \kappa(\mathbf{x}')}{2}.$$

(55)

We can prove analytically that with this assumption the peridynamic formulation converges to the classic local differential equation formulation at the limit of vanishing horizon. To do so let us consider the simple one-dimensional case with a uniform influence function. The pairwise interaction function of a point x with some point in its horizon is given by:

$$J(x) = \frac{(K(x+d) + K(x))}{\delta^2}\frac{(H(x+d) - H(x))}{|d|},$$

(56)

with d the distance between $\mathbf{x}$ and the interacting point. Writing Eq. (56) as a power series of order six, we get:

$$J(x) = \left(\frac{2\,sign(d)}{\delta^2}\right) \times \sum_{i=1}^{6}d^{i-1}\left(\frac{H^{(i)}(x)K(x)}{i!} + \left(\sum_{j=1}^{i-1}\frac{H^{(i-j)}(x)K^{(j)}(x)}{2\,(i-j)!j!}\right)\right),$$

(57)

where the superscript in parenthesis refers to the derivative order with respect to x. Integrating Eq. (57) over the entire horizon we get the change in moisture content:

$$\frac{\partial\theta}{\partial t} = \left(\frac{H^{(4)}K}{24} + \frac{H^{(3)}K^{(1)}}{12} + \frac{H^{(2)}K^{(2)}}{8} + \frac{H^{(1)}K^{(3)}}{12}\right)\delta^2$$

$$+ \left(\frac{H^{(6)}K}{1080} + \frac{H^{(5)}K^{(1)}}{360} + \frac{H^{(4)}K^{(2)}}{144} + \frac{H^{(3)}K^{(3)}}{108} + \frac{H^{(2)}K^{(4)}}{144} + \frac{H^{(1)}K^{(5)}}{360}\right)\delta^4$$

$$+ H^{(2)}K + H^{(1)}K^{(1)}.$$

(58)

Taking the limit of Eq. (58) when δ goes to zero reduces the peridynamic equation to the classic local model:

$$\lim_{\delta\to 0}\frac{\partial\theta}{\partial t} = K\frac{\partial^2 H}{\partial x^2} + \frac{\partial K}{\partial x}\frac{\partial H}{\partial x}.$$

(59)

Similarly, following the same approach we can prove that the peridynamic moisture flux reduces to the classic Darcy's equation at the limit of vanishing horizon. Rewriting the one-dimensional moisture flux equation (Eq. (20)) as follows:

$$q(\mathbf{x}) = -\int_0^\delta\int_p^\delta\frac{(K(x+d) + K(x))}{\delta^2}\frac{(H(x+d) - H(x))}{|d|}\,\mathrm{d}d\mathrm{d}p.$$

(60)

Evaluating the first integral after replacing the integrand by its series expansion (Eq. (57)), then performing a series expansion around p and evaluating the second integral leads to the following result:

$$q(\mathbf{x}) = KH^{(1)} + \sum_{i=1}^{5}\delta^i\left(\frac{2K^{(i)}H^{(i+1)}}{(i+1)!}\sum_{j=1}^{i}\frac{K^{(i-j+1)}H^{(j)}}{j!(i-j+1)!(i+2)}\right).$$

(61)

Taking the limit of Eq. (61) when δ goes to zero reduces the peridynamic equation to the classic Darcy's equation:

$$\lim_{\delta\to 0}q(\mathbf{x}) = K\frac{\partial H}{\partial x}.$$

(62)

5. Numerical implementation

Numerical implementation of the peridynamic model was based on a medium discretization into nodes using a regular grid. Fig. 4 shows a section of a discretized soil column in 1D and 2D respectively with a grid spacing of Δx and a horizon radius $\delta = m\Delta x$ with, where m is the horizon radius in multiples of grid lengths. Each node in the grid represents a volume of Δx for the 1D case, or Δx^2 for the 2D, and has a moisture content $\theta(x_n)$, an associated hydraulic potential $H(x_n)$ and a hydraulic conductivity $K(x_n)$.

It should be noted that there is no restriction on the type of grid used when discretizing the domain. The decision to use a regular grid was taken due to its simplicity and because only regular shapes will be modeled for this research. In fact, irregular grids are just as adequate, if not more helpful, when modeling complex geometries [30].
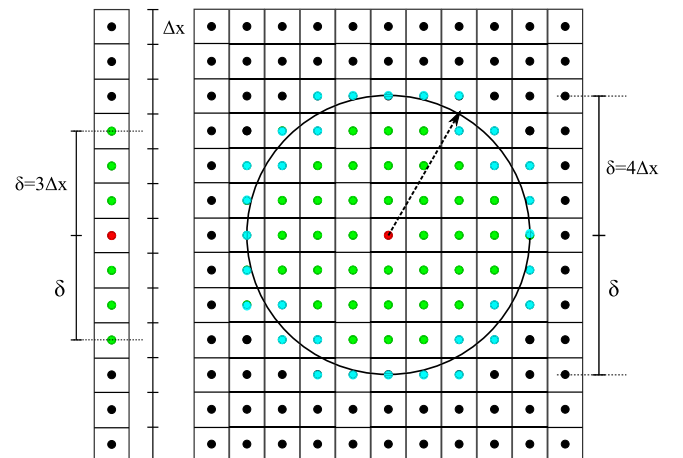

Fig. 4. 1D and 2D discrete representation of a peridynamic medium. Red point is the center of the horizon. Points in green and cyan are respectively fully and partially included in the horizon. (For interpretation of the references to colour in this figure legend, the reader is referred to the web version of this article.)

After setting the initial and boundary conditions, the discrete forms of the peridynamic equations of change in moisture content were explicitly integrated in time using the simple Euler method with a small time step. At the end of each time step, the hydraulic conductivity and the matric potential at every point in the domain are updated using the new moisture content values and the Van Genuchten hydraulic conductivity and water retention curves. Taking advantage of modern multi-core processors, the model code was written in C++ to run in parallel on shared memory machines using the OpenMP library.

Replacing κ in Eq. (12) by its expression for the one-dimensional case, Eq. (32) for a uniform influence function, and Eq. (32) for a linear influence function, and writing it in discrete form leads to the following discrete peridynamic equations for the evolution of moisture content for the cases of uniform and linear influence functions respectively:

$$\frac{\partial \theta(\mathbf{x_n})}{\partial t} = \sum_{\substack{p=n-m \\ p \neq n}}^{n+m} \frac{(K(\mathbf{x_n}) + K(\mathbf{x_p}))}{\delta^2 \|\mathbf{x_n x_p}\|} (H(\mathbf{x_p}) - H(\mathbf{x_n})) \Delta x, \tag{63}$$

$$\frac{\partial \theta(\mathbf{x_n})}{\partial t} = \sum_{\substack{p=n-m \\ p \neq n}}^{n+m} \left(1 - \frac{\|\mathbf{x_n x_p}\|}{\delta}\right) \frac{3(K(\mathbf{x_n}) + K(\mathbf{x_p}))}{\delta^2 \|\mathbf{x_n x_p}\|} (H(\mathbf{x_p}) - H(\mathbf{x_n})) \Delta x, \tag{64}$$

where the summation index p spans all the points belonging to the horizon of point $\mathbf{x_n}$.

As for the two-dimensional case, due to its increased computational cost a more efficient numerical scheme involving 2D convolutions was used to speed up the simulation. We will start by rewriting the 2D flow equation in a more concise manner:

$$\frac{\partial \theta_x}{\partial t} = \int_{\mathcal{H}_x} (K_x + K_{x'})(H_{x'} - H_x) A_{xx'} \, dVx', \tag{65}$$

where $A_{xx'}$ is obtained from Eqs. (50) and (54) describing the relationship between κ and K for the two-dimensional general anisotropic case using a uniform and linear influence functions respectively. $A_{xx'}$ is given by:

$$A_{xx'} = \frac{3(n+1)}{2n\pi\delta^2 \|\mathbf{xx'}\|} \left(\frac{\cos^2(\theta)}{n^2} + \sin^2(\theta)\right)^{-1}$$
$$\times \begin{cases} 1, & \text{Uniform influence function} \\ 4\left(1 - \frac{\|\mathbf{xx'}\|}{\delta}\right) & \text{Linear influence function} \end{cases}. \tag{66}$$

Expanding the integrand in Eq. (65), we get:

$$\frac{\partial \theta_x}{\partial t} = \int_{\mathcal{H}_x} K_x H_{x'} A_{xx'} \, dVx' - \int_{\mathcal{H}_x} K_x H_x A_{xx'} \, dVx'$$
$$+ \int_{\mathcal{H}_x} K_{x'} H_{x'} A_{xx'} \, dVx' - \int_{\mathcal{H}_x} K_{x'} H_x A_{xx'} \, dVx'. \tag{67}$$

Which is the following sum of two-dimensional convolutions with a circular kernel A with radius δ:

$$\frac{\partial \theta_x}{\partial t} = K_x(H * A) - K_x H_x(1 * A) + (KH) * A - H_x(K * A). \tag{68}$$

Because we are using a regular grid, and noting that $A_{xx'}$ depends only on $\|\mathbf{xx'}\|$ and θ and, therefore, could be represented by a matrix $A(2m+1, 2m+1)$, Eq. (68) is written in the following discrete form:

$$\frac{\partial \theta_{ij}}{\partial t} = K_{ij} \sum_{k=-m}^{m} \sum_{p=-m}^{m} H_{ab} A_{kp} \Delta x^2 - K_{ij} H_{ij} \sum_{k=-m}^{m} \sum_{p=-m}^{m} A_{kp} \Delta x^2$$
$$+ \sum_{k=-m}^{m} \sum_{p=-m}^{m} K_{ab} H_{ab} A_{kp} \Delta x^2 - H_{ij} \sum_{k=-m}^{m} \sum_{p=-m}^{m} K_{ab} A_{kp} \Delta x^2, \tag{69}$$

with $a = i + k$ and $b = j + p$.

At every time step of the simulation, each convolution in Eq. (69) is submitted and evaluated on one processor core. In addition, following the evaluation of the convolutions, the domain is split between all available cores where moisture content, matric potential, and hydraulic conductivity at each point are updated before the next time step.

Several functions exist for modeling the relationship between the soil moisture content and matric potential and for calculating the unsaturated hydraulic conductivity as a function of the moisture content and the saturated hydraulic conductivity. For the current implementation we opted for the Van Genuchten model [31] for matric potential and hydraulic conductivity given by the following equations:

$$\theta(H) = \theta_r + \frac{\theta_s - \theta_r}{\left[1 + (\alpha|H|)^n\right]^{1-1/n}}, \tag{70}$$

$$K(\theta) = K_s \left(\frac{\theta - \theta_r}{\theta_s - \theta_r}\right)^{\frac{1}{2}} \left\{1 - \left[1 - \left(\frac{\theta - \theta_r}{\theta_s - \theta_r}\right)^{\frac{n}{n-1}}\right]^{\frac{n-1}{n}}\right\}^2, \tag{71}$$

where θ_s and θ_r are the saturation and residual volumetric water content respectively. Also, K_s is the soil hydraulic conductivity at saturation, α is related to the inverse of the air entry pressure, and n is a parameter related to the soil pore size distribution. Rearranging Eq. (70) we get the matric potential as a function of the moisture content:

$$H(\theta) = -\frac{1}{\alpha} \left[\left(\frac{\theta_s - \theta_r}{\theta - \theta_r}\right)^{\frac{n}{n-1}} - 1\right]^{\frac{1}{n}}. \tag{72}$$

6. Model validation

In order to validate the proposed model, and analyze the effects that the horizon radius (δ), the density of points per horizon radius (m), and the type of influence function (uniform or linear) have on the performance of the model, several 1D and 2D scenarios are simulated. Due to the lack of an analytical solution of the flow problem, the same scenarios are also simulated using the finite element models HYDRUS-1D and HYDRUS 2D/3D [32,33] that solve the classic Richard's equation in one dimension and two dimensions respectively, and their results are used as a benchmark for evaluating the accuracy of the peridynamic flow model.

The simulations are divided into three groups. The first group includes 1D scenarios that simulate drainage from a saturated soil column for various horizon radius values, and various point density values for each radius. The simulations were performed using a uniform influence function, and repeated using a linear influence function. Groups two and three are 2D scenarios. Group 2 simulates moisture redistribution within a horizontal soil layer having an area with a higher moisture content than the rest of the layer. The third group is scenarios of drainage from a vertical soil column with a moisture content initially at saturation. The soil in the first group has homogeneous properties, whereas the soil in the second group is composed of two soil types. 2D simulations were performed assuming isotropy, and then repeated assuming anisotropy of the hydraulic conductivity; they were also performed twice, using a uniform influence function in one, and a linear influence function in the other.

6.1. One-dimensional scenarios

In these scenarios we simulate drainage of a vertical soil column from saturation. The vertical soil column is 300 cm long. Initially the entire soil column is at saturation. The top boundary at

$x = 300$ cm is a no flow boundary condition. The bottom boundary is maintained at saturation, simulating the level of the water table at $x = 0$ cm.

Table 1 lists the different horizon radii and m values used, along with the corresponding grid spacing. Table 2 lists the soil parameters for the Van Genuchten model for matric potential and hydraulic conductivity for the soil used.

In HYDRUS-1D the column is simulated using the Van Genuchten soil model, and a top boundary condition of zero flux. The bottom boundary is maintained at saturation and, initially, all the soil profile is set to saturation moisture content. Grid length is set to 0.5 cm in order to remain within the maximum number of nodes of the program. Conversion criteria were set to 1E-5 for absolute change in moisture content and to 0.01 cm for absolute change in matric potential.

For the peridynamic model, the soil is initially set at saturation moisture content. Because of the nonlocal nature of the formulation, the bottom boundary condition is simulated by adding an additional number of nodes from $x = 0$ cm to $x = -\delta$. The lower boundary nodes are maintained at saturation moisture content for the duration of the simulation. The time step used for the drainage scenarios is 1E-6 days.

Fig. 5 is a plot of the moisture profile of the drainage scenario recorded time at 1 day, 3 day and 10 days. The solid lines are the results using the classic formulation modeled using HYDRUS-1D. Overlaid in squares and triangles are the plots using the peridynamic formulation for the uniform and linear influence functions respectively for a horizon radius $\delta = 1$ cm and a point density value $m = 4$. Following a visual inspection of the plots we observe a very good agreement between the results of the peridynamic model and the classic model.

In order to obtain a more quantitative evaluation of the level of agreement between both methods, we will analyze more closely the results at 1 day. Specifically, we will examine the effects the values of the horizon radius (δ), the point density (m) and the shape of the influence function (*uniform* or *linear*) have on the relative difference between the results of the peridynamic model and HYDRUS-1D for two variables: the value of the surface moisture content and the total amount of moisture that exited the profile. The relative difference is calculated as follows:

$$rd(\mathbf{x}) = 100 \frac{\theta_{peri}(\mathbf{x}) - \theta_{classic}(\mathbf{x})}{\theta_{classic}(\mathbf{x})}. \tag{73}$$

Figs. 6 and 7 are plots of the relative difference of the surface moisture content versus the point density value (m) for various horizon radii ($\delta = 1, 3, 4, 5$ cm) using a uniform influence function and a linear influence function respectively. We observe that with increasing values of m, the relative difference curve for each

Table 1
Grid size for the various horizon radii (δ) and point densities (m) used in the one-dimensional scenarios.

| $\delta \setminus m$	1	3	4	5
2	0.500	1.500	2.0	2.50
4	0.250	0.750	1.0	1.25
5	0.200	0.600	0.8	1.00
8	0.125	0.375	0.5	0.625

Table 2
Van Genuchten soil parameters for the one-dimensional scenarios.

| θ_s (–)	θ_r (–)	K_s (cm/day)	α (cm^{-1})	n (–)
0.430	0.078	24.96	0.036	1.56
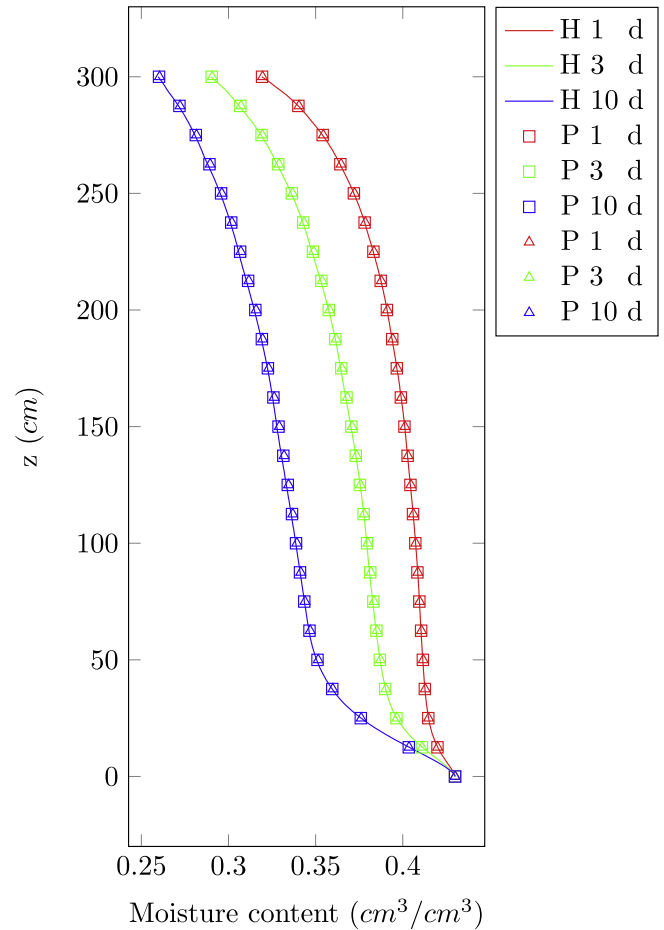
Fig. 5. Drainage scenario: Moisture profile at 1, 3, and 10 days. HYDRUS-1D simulation results plotted as solid lines. Peridynamic simulation results for $\delta = 1$ cm, $m = 4$. Uniform influence function results plotted as squares, linear as triangles; only every 50 points are plotted for visibility.
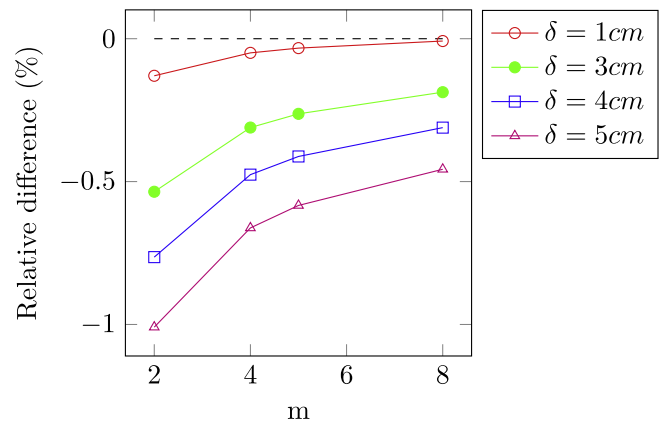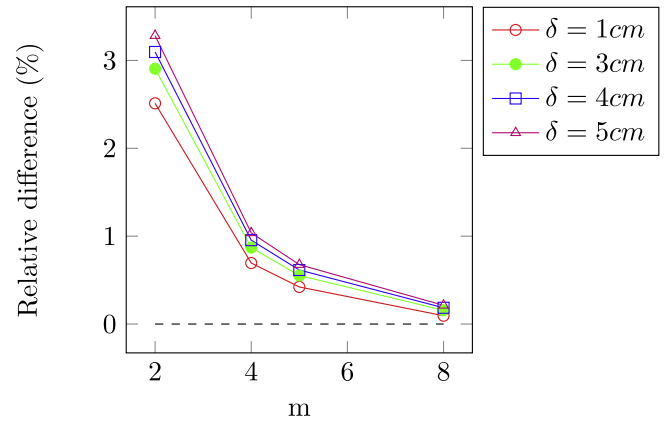

Fig. 6. Drainage scenario: effect of m on the relative difference (%) for soil surface moisture content at 1 day between HYDRUS-1D and the peridynamic simulation using a uniform influence function. For each horizon radius the relative difference decreases with increasing point density. Also, relative difference curves of smaller horizon radii are closer to 0%.

horizon radius (δ) converges to a limit value with smaller relative difference. This behavior is expected; as the number of points within a horizon increases, the distribution of moisture content is sampled more accurately and its influence on the change of moisture content at the center of the horizon is better represented.
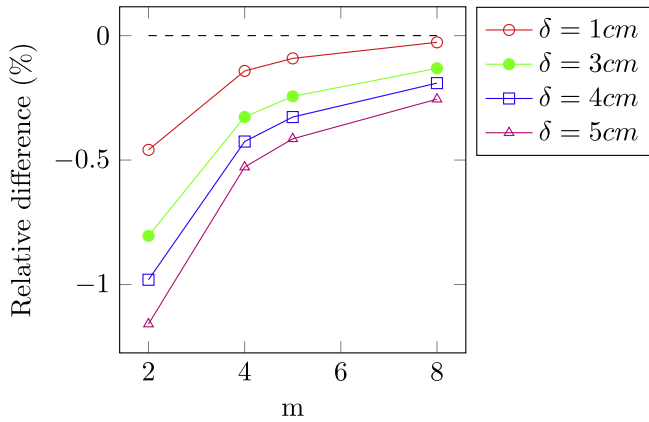
Fig. 7. Drainage scenario: effect of *m* on the relative difference (%) for soil surface moisture content at 1 day between HYDRUS-1D and the peridynamic simulation using a linear influence function. For each horizon radius the relative difference decreases with increasing point density. Also, relative difference curves of smaller horizon radii are closer to 0%.

Fig. 9. Drainage scenario: effect of *m* on the relative difference (%) for total amount of drained moisture at 1 day between HYDRUS-1D and the peridynamic simulation using a linear influence function. For each horizon radius the relative difference decreases with increasing point density. Also, relative difference curves of smaller horizon radii are closer to 0%.

The same trend is observed in Figs. 8 and 9, where the relative difference of the total moisture that drained out of the profile is plotted against *m* for the same horizon radii, using uniform and linear influence functions respectively.

The results also indicate that as the horizon radius (δ) decreases the performance of the model increases. Larger horizon radii (δ) lead to an overestimation of the surface moisture content, and an underestimation of the total amount of drained moisture. With decreasing horizon radii, the relative difference moves towards a smaller value. This is evident in Figs. 6–9 where the curves of smaller horizons fall closer to the zero relative difference line. We attribute this to the fact that as the horizon radius decreases, the influence of points closer to the center of the horizon increases and the model becomes more localized and closer to the classic local formulation.

6.2. Two-dimensional scenarios

These scenarios are divided into two groups. The first group is scenarios of moisture redistribution within a horizontal soil layer having an area with a higher moisture content than the rest of the layer. The second group is scenarios of drainage from a vertical soil column with a moisture content initially at saturation. The soil in the first group has homogeneous properties, whereas the soil in the second group is composed of two soil types.

In each group, the simulations were performed assuming isotropy, and then repeated assuming anisotropy of the hydraulic conductivity. In addition, every simulation was performed twice, using a uniform influence function in one, and a linear influence function in the other. All the peridynamic simulations were performed using a horizon radius $\delta = 1$ cm and a point density value $m = 4$ yielding a grid size $\Delta x = 0.25$ cm. The choice δ and m was made by taking into consideration the results of the convergence analysis performed in developing the peridynamic flow model in one dimension, and the computational resources required for running the simulations.

The properties of the various soils used in the simulations such as residual moisture content, moisture content at saturation, and the saturated hydraulic conductivities, along with the Van Genuchten model parameters for these soils, are listed in Table 3.
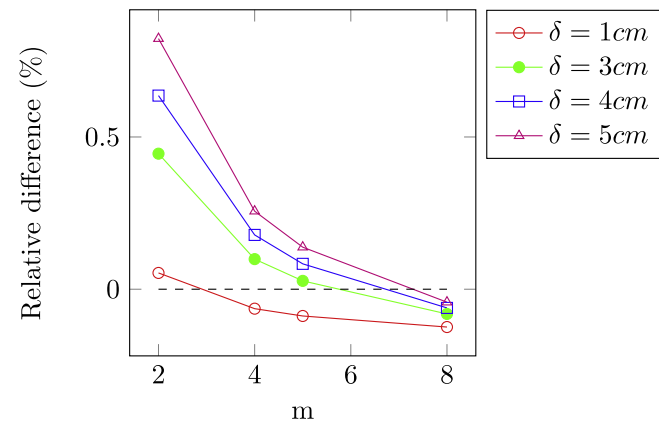
6.2.1. Moisture redistribution scenarios

These examples simulate the redistribution of moisture within a two-dimensional horizontal layer of soil. The soil layer is 100 cm long by 100 cm wide. The soil layer is divided into two zones. Zone One is a 30 cm long by 30 cm wide in the middle of the soil layer with the lower left corner located at coordinates $(35, 35)$ and the upper right corner located at coordinates $(65, 65)$. Zone Two is the soil layer excluding Zone One. Soil properties in both zones are identical. Initially, the soil in Zone One is at saturation moisture content 0.43%, and the soil in Zone Two is at 0.25%. The boundary conditions at the edges of the soil layer are no flow boundary conditions. We simulated two variants of this example. In the first variant, we used soil S1 that has an isotropic hydraulic conductivity; in the second, we used soil S2 that has an anisotropic hydraulic conductivity, with the major conductivity directions parallel to the model axis.

Fig. 8. Drainage scenario: effect of *m* on the relative difference (%) for total amount of drained moisture at 1 day between HYDRUS-1D and the peridynamic simulation using a uniform influence function. For each horizon radius the relative difference decreases with increasing point density. Also, relative difference curves of smaller horizon radii are closer to 0%.

Table 3
Van Genuchten soil parameters for two-dimensional scenarios.

SoilID	θ_s (−)	θ_r (−)	Ks_1 (cm/day)	Ks_2 (cm/day)	α (cm^{-1})	n (−)
S1	0.430	0.078	12.48	12.48	0.036	1.56
S2	0.430	0.078	24.96	12.48	0.036	1.56
S3	0.430	0.078	24.96	24.96	0.036	1.56
S4	0.430	0.078	12.48	6.24	0.036	1.56

In HYDRUS 2D/3D, the layer is simulated using the Van Genuchten soil model, with all boundary conditions set to zero flux. Initially, nodes in Zone One are set to saturation moisture content, and all the other nodes are set to a moisture content of 0.25%. Grid length is set to 0.5 cm in order to remain within the maximum number of nodes of the program. Conversion criteria were set to 1E-5 for absolute change in moisture content and to 0.01 cm for absolute change in matric potential.

For the peridynamic model, zero flux boundary conditions were simulated by using periodic boundary conditions. Because of the symmetry of the problem, periodic and no flow boundary conditions are equivalent. The moisture content for soil volumes in Zone One were initially set to saturation moisture content, and the remaining were set to a moisture content of 0.25%. The time step used for these scenarios is 1E-5 h.

Isotropic conductivity. Fig. 10 is an image of the moisture content distribution of the isotropic redistribution scenario at 2 h simulated using HYDRUS 2D/3D. It is clear from Figs. 11 and 12 that for both influence function types, the relative difference between the peridynamic and classic models is very small, and varies between around −0.1%, up to about 0.4% for the uniform influence function,
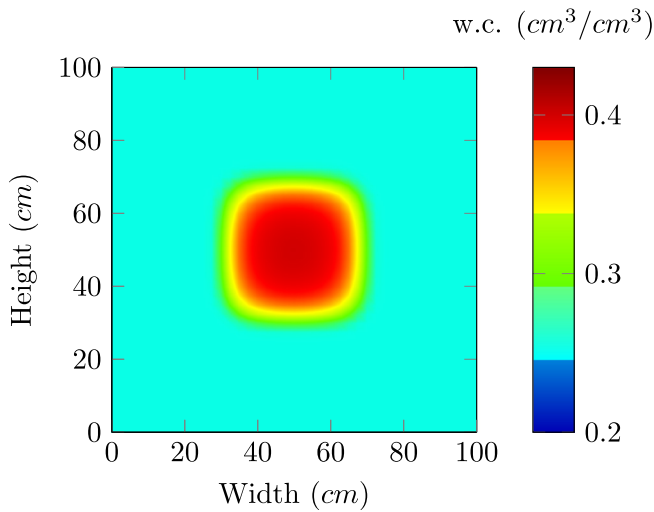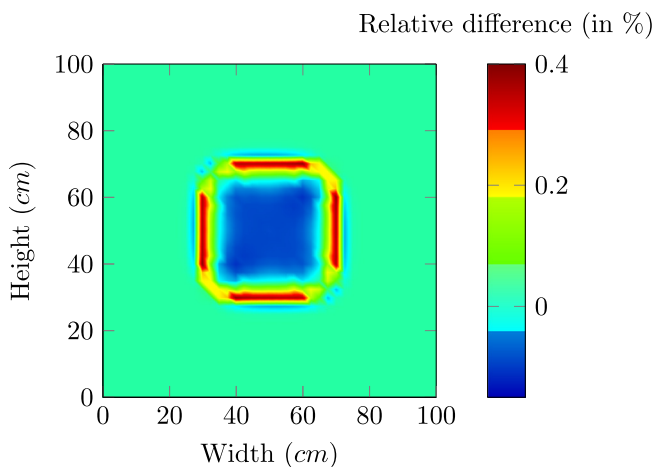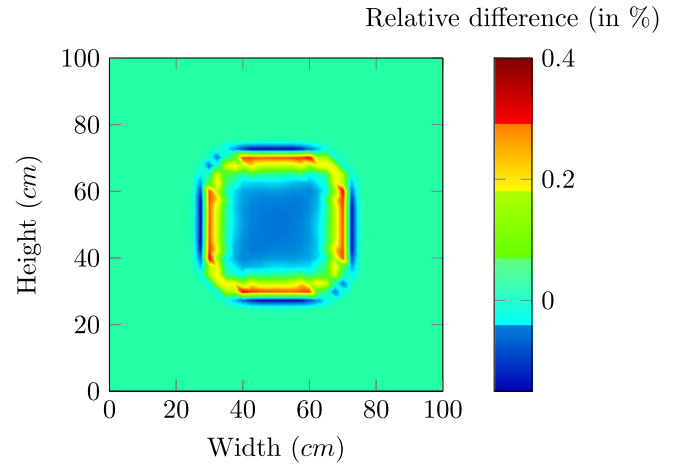

Fig. 12. Redistribution scenario, isotropic soil: relative difference (in %) of moisture content between the peridynamic model results and the classic model HYDRUS at 2 h. Linear influence function, $\delta = 1$ cm, and a point density value $m = 4$.

Fig. 10. Redistribution scenario, isotropic soil: hydrus simulation results for moisture content at 2 h.

Fig. 11. Redistribution scenario, isotropic soil: relative difference (in %) of moisture content between the peridynamic model results and the classic model HYDRUS at 2 h. Uniform influence function, $\delta = 1$ cm, and a point density value $m = 4$.

and up to 0.3% for the linear influence function. We notice that at the center of Zone One, the peridynamic model slightly underestimates the moisture content. As we move away from the center, the relative difference changes very slowly until we get closer to the edges of Zone One, where it increases sharply and becomes positive, then sharply decreases back to a small negative value before it tapers off at zero.

The fact that these sharp changes in relative difference happen over a small distance makes them less problematic and reduces their bearing on the performance of the model. Nevertheless, they are better understood when we notice that they coincide at the front separating the saturated soil from the soil at a lower moisture content. In this region, the moisture gradient is very large, and even small variations in its location and shape from one model to another may lead to large variations in moisture content at points within the front.

These variations between the classic and the peridynamic models can be attributed to the nature of these models, specifically the local versus non-local aspects of the formulations. To illustrate, let us go through the process of moisture redistribution scenario. At the beginning of the simulation, the soil has a sharp drop in moisture at the interface between Zone One and Zone Two. As time goes by, moisture flows from Zones One into Zone Two, which leads to an increase of the moisture content in Zone Two and a decrease in Zone One near the interface. Consequently, the interface zone widens and the moisture gradient becomes smaller. In the classic local formulation, this exchange happens over an infinitesimal distance; whereas, in the nonlocal peridynamic framework, moisture exchange happens over the entire radius of the horizon. This means that moisture is exchanged from one side of the front to the other, between points located further away from the front. This leads to more moisture moving from one side of the interface to the other side, which explains the observed relative differences.

Although this behavior is observed in both peridynamic simulations, some differences exist between the results obtained using a uniform influence function and those obtained using a linear influence function. The simulation using the uniform type underestimated the moisture content inside Zone One, and overestimated it near the front in Zone Two when compared to the results from the linear influence function.

These differences between the uniform and linear influence functions are attributed to the shape of the function. Despite the fact that we used the same horizon radius in both simulations, the uniform influence function treats all the points within a

horizon equally, whereas a linear influence function favors more points that are near the center at the expense of points further away. This preference for points closer to the center makes the behavior of a peridynamic model with a linear influence function less nonlocal and closer to the classic local model.

Anisotropic conductivity. Fig. 13 is an image of the moisture content distribution of the anisotropic redistribution scenario at 2 h simulated using HYDRUS 2D/3D. From Figs. 14 and 15 we notice that the values of the relative difference are acceptable and range between −0.2% and 0.7%. Similarly to the results from the simulations of isotropic soils, we notice that at the center of Zone One, the model slightly underestimates the moisture content. As we move away from the center, the relative error changes very slowly until we get closer to the edges of Zone One, where the relative difference increases sharply before it reverses in direction and tapers off at zero.

However, when compared to the simulations of the isotropic soil, these results exhibit some very clear differences in the relative difference. The first is the difference in magnitude of the relative difference between the major flow axes, where it is higher in the direction of faster flow. The second is that the results of
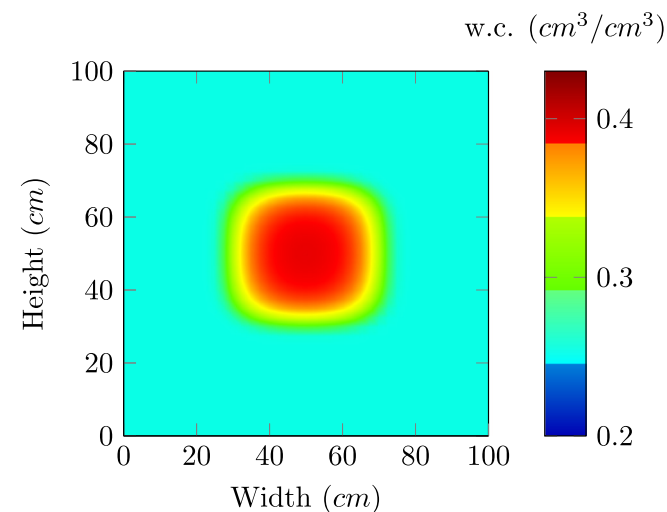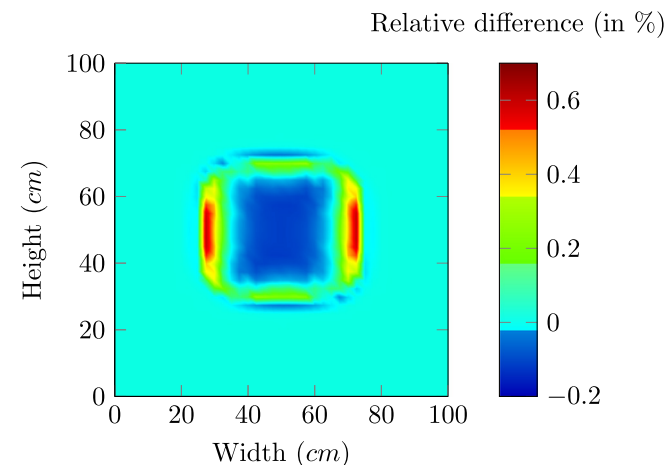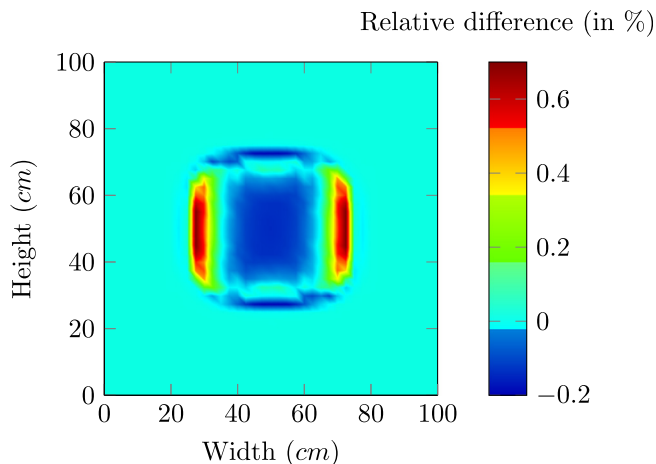

Relative difference (in %)

Fig. 15. Redistribution scenario, anisotropic soil: relative difference (in %) of moisture content between the peridynamic model results and the classic model HYDRUS at 2 h. Linear influence function, $\delta = 1$ cm, and a point density value $m = 4$.

the simulation using a linear influence function show even higher relative difference along this direction, and a reduction in the relative difference in the direction of slower flow, compared to the results using the uniform influence function.

We attribute the model's deviation in behavior from the isotropic soil simulations to a combination of factors. The first factor is related to the Euler scheme we used to integrate the simulation forward in time. This naive numerical method requires a very small time step to give accurate results, which we used. However, no matter how small the error is, it remains proportional to the hydraulic conductivity, and it effectively translates into a proportional increase in the conductivity.

The second factor in the model's deviation is related to the medium's anisotropy. As a result of this anisotropy, the error in the direction of the fast flow will be larger than the error in the direction of the slow flow. This asymmetry in the error leads to an effective increase in the conductivity that is also asymmetric and highest along the fast flow direction. Consequently, more moisture flows from Zone One towards the left and right fronts, leaving the center with a lower than expected moisture content, which in turn slows the flow in the other direction and prevents higher relative differences at the top and bottom front.

This behavior is even more pronounced when we use a linear influence function, which is peculiar since the more local behavior of the linear influence function suggests that the results should be closer to the classic model. However, Fig. 15 shows a stronger asymmetry, with a higher increase in relative difference at the left and right fronts, and a higher decrease in relative difference at the top and bottom fronts. One potential explanation is that because of the more local behavior and the fact that a linear function favors more points closer to the center, the linear influence function better captures the effects of the numerical errors, whereas the uniform influence function smears this effect over the entire horizon by acting as a low pass filter.

6.2.2. Drainage scenarios – heterogeneous soil

The following examples simulate the drainage of moisture from a two-dimensional vertical layer of soil. The soil layer is 100 cm long by 100 cm wide, and is divided into three vertical zones. Zone Two is 100 cm long by 30 cm wide in the middle of the soil layer with the lower left corner located at coordinates $(35, 0)$ and the upper right corner located at coordinates $(65, 100)$. Zone One and Zone Three are respectively at the left and right of Zone Two. Zone One and Zone Three have identical soils, whereas the soil in Zone

w.c. (cm^3/cm^3)

Fig. 13. Redistribution scenario, anisotropic soil: hydrus simulation results for moisture content at 2 h.

Relative difference (in %)

Fig. 14. Redistribution scenario, anisotropic soil: relative difference (in %) of moisture content between the peridynamic model results and the classic model HYDRUS at 2 h. Uniform influence function, $\delta = 1$ cm, and a point density value $m = 4$.

Two has a faster hydraulic conductivity. Initially, the soil is at saturation moisture content (0.43%). The left, right, and top boundary conditions are no flow boundary conditions, and the bottom boundary is maintained at saturation. We simulated two variants of this example. In the first variant, we used soil S1, in Zone One and Zone Three, and soil S3 in Zone Two, all of which have an isotropic hydraulic conductivity. In the second variant we replaced soils S1 and S3 by soils S4 and S2 respectively. These soils have an anisotropic hydraulic conductivity, with the major conductivity directions parallel to the model axis.

In HYDRUS 2D/3D, the layer is simulated using the Van Genuchten soil model. The left, right, and top boundary conditions are set to zero flux, while the bottom boundary is maintained at saturation. Soil elements were assigned their respective type depending on their location. At time zero all nodes were set to saturation moisture content. Grid length is 0.5 cm in order to remain within the maximum number of nodes of the program. Convergence criteria were set to 1E-5 for absolute change in moisture content and to 0.01 cm for absolute change in matric potential.

For the peridynamic model, zero flux boundary conditions were assigned to the top, left and right boundaries. Because of the non-local nature of the formulation, the bottom boundary condition was simulated by adding an additional number of nodes from $x = 0$ cm to $x = -\delta$. The lower boundary nodes were maintained at saturation moisture content for the duration of the simulation. Moisture content was set initially to saturation everywhere, and the soil volumes were assigned their respective soil types. The time step used for these scenarios was 1E-6 days.

Isotropic conductivity. Fig. 16 is an image of the moisture content distribution of the isotropic drainage scenario at 0.2 days simulated using HYDRUS 2D/3D. As in our previous analysis, we will look at the relative difference of the moisture content between the results of the peridynamic model and the classic model to evaluate the level of agreement between both models and investigate the impact of the type of the influence function on the performance of the model. Figs. 17 and 18 are the images of the relative difference at 0.2 days for the uniform and linear influence functions respectively.

We note from these results that for both influence function types, the relative difference between the peridynamic and the classic models is small, and does not exceed −0.275%, with the results of the simulation using a linear influence function yielding smaller areas with large relative differences.
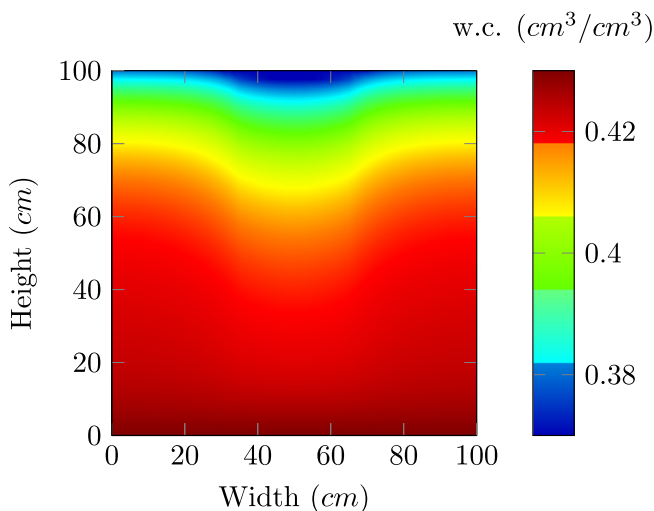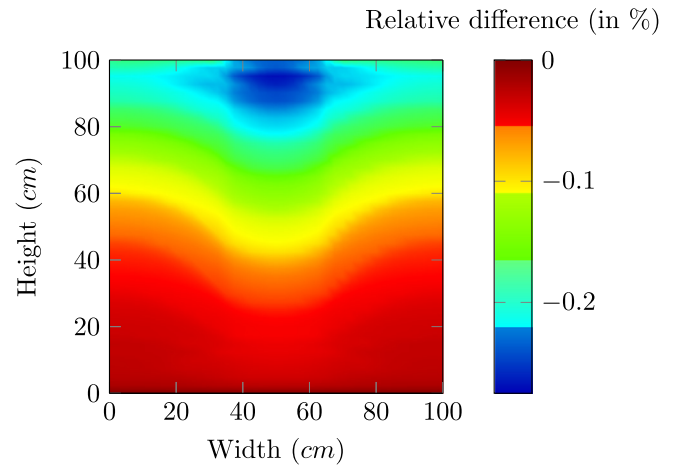

Fig. 17. Drainage scenario, isotropic soil: relative difference (in %) of moisture content between the peridynamic model results and the classic model HYDRUS at 0.2 days. Uniform influence function, $\delta = 1$ cm, and a point density value $m = 4$.
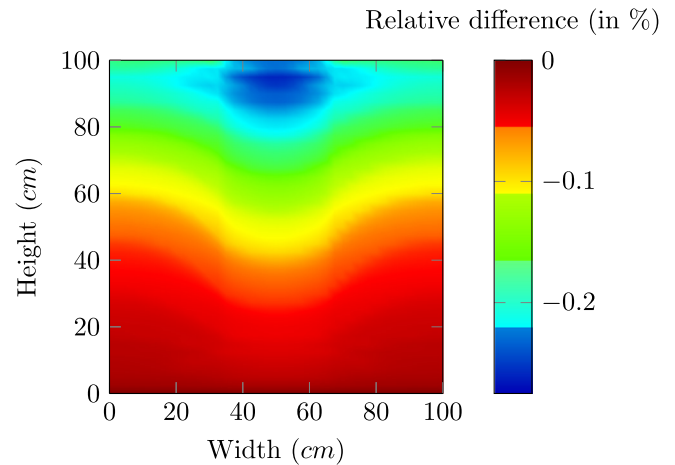

Fig. 18. Drainage scenario, isotropic soil: relative difference (in %) of moisture content between the peridynamic model results and the classic model HYDRUS at 0.2 days. Linear influence function, $\delta = 1$ cm, and a point density value $m = 4$.

Fig. 16. Drainage scenario, isotropic soil: hydrus simulation results for moisture content at 0.2 days.

We also note an interesting feature near the top boundary where the relative difference decreases. This feature is attributed to a reduced conductivity compared to the rest of the domain which produces a lower moisture flow out of the soil near the boundary and leads to the high relative differences observed just below the boundary. This reduced conductivity is the result of the assumptions made when deriving the relationship between the peridynamic and the classic conductivity – specifically, the assumption that a point interacts with a full horizon, which is not the case for points located less than a horizon radius away from the boundary.

Anisotropic conductivity Fig. 19 is an image of the moisture content distribution of the anisotropic drainage scenario at 0.2 days simulated using HYDRUS 2D/3D. We note from the results in Figs. 20 and 21 that for both influence function types, the relative difference between the peridynamic and the classic models is small, and does not exceed −0.2% for the uniform influence function, and −0.16% for the linear influence function.

The same feature that is observed near the top boundary in the isotropic case is also present, but it is more stretched in the direction of the higher conductivity. We attribute this to the higher
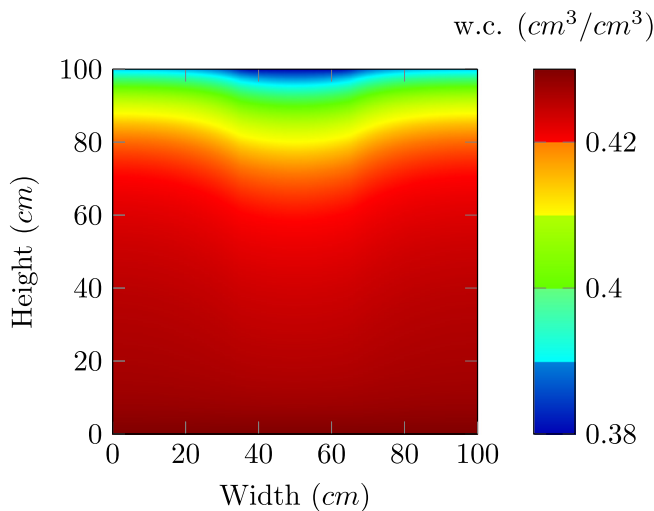
Fig. 19. Drainage scenario, anisotropic soil: hydrus simulation results for moisture content at 0.2 days.
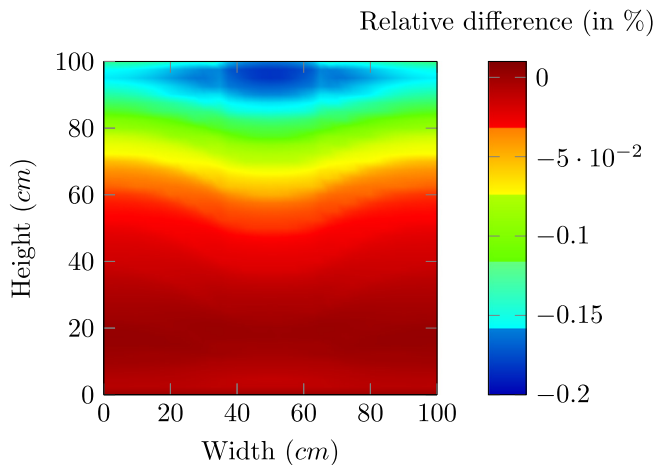

Fig. 20. Drainage scenario, anisotropic soil: relative difference (in %) of moisture content between the peridynamic model results and the classic model HYDRUS at 0.2 days. Uniform influence function, $\delta = 1$ cm, and a point density value $m = 4$.
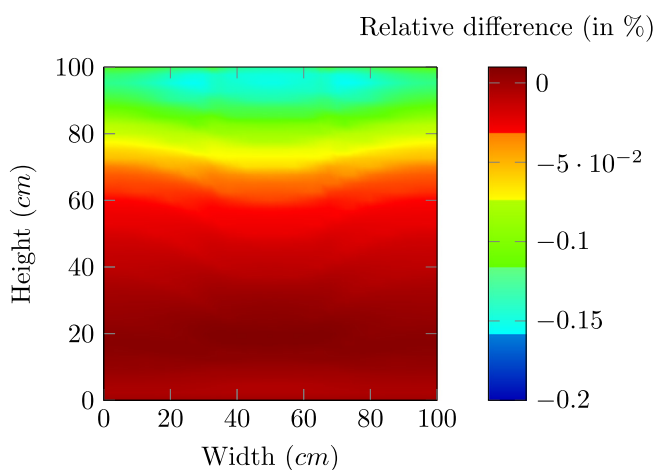

Fig. 21. Drainage scenario, anisotropic soil: relative difference (in %) of moisture content between the peridynamic model results and the classic model HYDRUS at 0.2 days. Linear influence function, $\delta = 1$ cm, and a point density value $m = 4$.

conductivity of the soil in Zone Two that is draining faster and pulling more water in from Zone One and Zone Three, which also have a higher conductivity in the horizontal direction that leads to the mobilization of an additional horizontal flow at that depth which extends the region of lower moisture content laterally.

7. Conclusion

In this paper we derived a nonlocal derivative free alternative of the Richards equation. We replaced the deferential flow equation by an integral functional, where the absence of spacial derivative allows for the simulation of domains with internal evolving singularities such as desiccation cracks, a feature of soils with a high shrink/swell potential. Expressions relating the peridynamic hydraulic conductivity to the measurable classic hydraulic conductivity were derived for problems in one- and two-dimensions including heterogeneous and anisotropic soils.

Using the derived model, we simulated scenarios of drainage and moisture redistributions in one- and two-dimensions. We repeated the same simulation using the classic local formulation using HYDRUS, a finite element model that solves the classic Richards equation [32,33]. The results of both formulations were compared and show a good level of agreement. It is important to mention that the simulated validation scenarios did not include soil domains undergoing cracking. Validation of the model for the case of cracking soils is the subject of current research and will be presented in a subsequent paper.

References

[1] Davidson SE, Page JB. Factors influencing swelling and shrinking in soils. Soil Sci Soc Am J 1956;20(3):320–4. http://dx.doi.org/10.2136/sssaj1956.03615995002000030007x.
[2] Dinka TM. Review paper: challenges and limitations in studying the shrink–swell and crack dynamics of vertisol soils. Open J Soil Sci 2012;02(02):82–90. http://dx.doi.org/10.4236/ojss.2012.22012.
[3] Braudeau E, Mohtar RH. Modeling the swelling curve for packed soil aggregates using the pedostructure concept. Soil Sci Soc Am J 2006;70(2):494. http://dx.doi.org/10.2136/sssaj2004.0211.
[4] Chertkov VY. Modelling cracking stages of saturated soils as they dry and shrink. Eur J Soil Sci 2002;53(1):105–18. http://dx.doi.org/10.1046/j.1365-2389.2002.00430.x.
[5] Greco R. Preferential flow in macroporous swelling soil with internal catchment: model development and applications. J Hydrol 2002;269(3–4):150–68. http://dx.doi.org/10.1016/S0022-1694(02)00215-9.
[6] Jarvis NJ. A review of non-equilibrium water flow and solute transport in soil macropores: principles, controlling factors and consequences for water quality. Eur J Soil Sci 2007;58(3):523–46. http://dx.doi.org/10.1111/j.1365-2389.2007.00915.x.
[7] Greve A, Andersen MS, Acworth RI. Investigations of soil cracking and preferential flow in a weighing lysimeter filled with cracking clay soil. J Hydrol 2010;393(1):105–13. http://dx.doi.org/10.1016/j.jhydrol.2010.03.007.
[8] Kosmas C, Moustakas N, Kallianou C, Yassoglou N. Cracking patterns, bypass flow and nitrate leaching in greek irrigated soils. Geoderma 1991;49(1–2):139–52. http://dx.doi.org/10.1016/0016-7061(91)90097-D.
[9] Harris G, Nicholls P, Bailey S, Howse K, Mason D. Factors influencing the loss of pesticides in drainage from a cracking clay soil. J Hydrol 1994;159(1–4):235–253, http://dx.doi.org/. http://dx.doi.org/10.1016/0022-1694(94)90259-3.
[10] Lin H, Mcinnes K. Water-flow in clay soil beneath a tension infiltrometer. Soil Sci 1995;159(6):375–82. http://dx.doi.org/10.1097/00010694-199506000-00002.
[11] Arnold JG, Potter KN, King KW, Allen PM. Estimation of soil cracking and the effect on surface runoff in a texas blackland prairie watershed. Hydrol Process 2005;19(3):589–603. http://dx.doi.org/10.1002/hyp.5609.
[12] Smith R, Raine S, Minkevich J. Irrigation application efficiency and deep drainage potential under surface irrigated cotton. Agric Water Manage 2005;71(2):117–30. http://dx.doi.org/10.1016/j.agwat.2004.07.008.
[13] Wang J-J, Zhu J-G, Mroueh H, Chiu CF. Hydraulic fracturing of rock-fill dam. Int J Multiphys 2007;1(2):199–219. http://dx.doi.org/10.1139/t90-064.
[14] Albrecht B, Benson C. Effect of desiccation on compacted natural clays. J Geotech Geoenviron Eng 2001;127(1):67–75. http://dx.doi.org/10.1061/(ASCE)1090-0241(2001)127:1(67).
[15] Dixon D, Chandler N, Graham J, Gray MN. Two large-scale sealing tests conducted at atomic energy of Canada's underground research laboratory: the buffer-container experiment and the isothermal test. Can Geotech J 2002;39(3):503–18. http://dx.doi.org/10.1139/t02-012.

[16] Silling S. Reformulation of elasticity theory for discontinuities and long-range forces. J Mech Phys Solids 2000;48(1):175–209. http://dx.doi.org/10.1016/S0022-5096(99)00029-0.

[17] Silling S, Lehoucq R. Peridynamic theory of solid mechanics. In: Advances in applied mechanics, vol. 44. Elsevier; 2010. p. 73–168. http://dx.doi.org/10.1016/S0065-2156(10)44002-8.

[18] Katiyar A, Foster JT, Ouchi H, Sharma MM. A peridynamic formulation of pressure driven convective fluid transport in porous media. J Comput Phys 2014;261:209–29. http://dx.doi.org/10.1016/j.jcp.2013.12.039.

[19] Indelman P, Abramovich B. Nonlocal properties of nonuniform averaged flows in heterogeneous media. Water Resour Res 1994;30(12):3385–93. http://dx.doi.org/10.1029/94WR01782.

[20] Neuman SP, Orr S. Prediction of steady state flow in nonuniform geologic media by conditional moments: exact nonlocal formalism, effective conductivities, and weak approximation. Water Resour Res 1993;29(2):341–64. http://dx.doi.org/10.1029/92WR02062.

[21] Neuman SP. Trends, prospects and challenges in quantifying flow and transport through fractured rocks. Hydrogeol J 2005;13(1):124–47. http://dx.doi.org/10.1007/s10040-004-0397-2.

[22] Tartakovsky DM, Neuman SP, Lu Z. Conditional stochastic averaging of steady state unsaturated flow by means of kirchhoff transformation. Water Resour Res 1999;35(3):731–45. http://dx.doi.org/10.1029/1998WR900092.

[23] Tartakovsky DM, Neuman SP. Transient effective hydraulic conductivities under slowly and rapidly varying mean gradients in bounded three-dimensional random media. Water Resour Res 1998;34(1):21–32. http://dx.doi.org/10.1029/97WR01965.

[24] Tartakovsky DM, Neuman SP. Transient flow in bounded randomly heterogeneous domains: 1. exact conditional moment equations and recursive approximations. Water Resour Res 1998;34(1):1–12. http://dx.doi.org/10.1029/97WR02118.

[25] Tartakovsky DM, Neuman SP. Transient flow in bounded randomly heterogeneous domains: 2. localization of conditional mean equations and temporal nonlocality effects. Water Resour Res 1998;34(1):13–20. http://dx.doi.org/10.1029/97WR02117.

[26] Bobaru F, Duangpanya M. The peridynamic formulation for transient heat conduction. Int J Heat Mass Transfer 2010;53(19–20):4047–59. http://dx.doi.org/10.1016/j.ijheatmasstransfer.2010.05.024.

[27] Bobaru F, Hu W. The meaning, selection, and use of the peridynamic horizon and its relation to crack branching in brittle materials. Int J Fract 2012;176(2):215–22. http://dx.doi.org/10.1007/s10704-012-9725-z.

[28] Seleson P, Parks M. On the role of the influence function in the peridynamic theory. Int J Multiscale Comput Eng 2011;9(6):689–706. http://dx.doi.org/10.1615/IntJMultCompEng.2011002527.

[29] Kilic B, Madenci E. Peridynamic theory for thermomechanical analysis. IEEE Trans Adv Packag 2010;33(1):97–105. http://dx.doi.org/10.1109/TADVP.2009.2029079.

[30] Silling S, Askari E. A meshfree method based on the peridynamic model of solid mechanics. Comput Struct 2005;83(17–18):1526–35. http://dx.doi.org/10.1016/j.compstruc.2004.11.026.

[31] Van Genuchten MT. A closed-form equation for predicting the hydraulic conductivity of unsaturated soils. Soil Sci Soc Am J 1980;44(5):892–8. http://dx.doi.org/10.2136/sssaj1980.03615995004400050002x.

[32] Simunek J, Sejna M, Van Genuchten M. The HYDRUS-1D software package for simulating the one-dimensional movement of water, heat, and multiple solutes in variably-saturated media, University of California, Riverside, Research reports 240..

[33] Simunek J, Van Genuchten MT, Sejna M. The hydrus software package for simulating the two-and three-dimensional movement of water, heat, and multiple solutes in variably-saturated media, Technical manual 1.